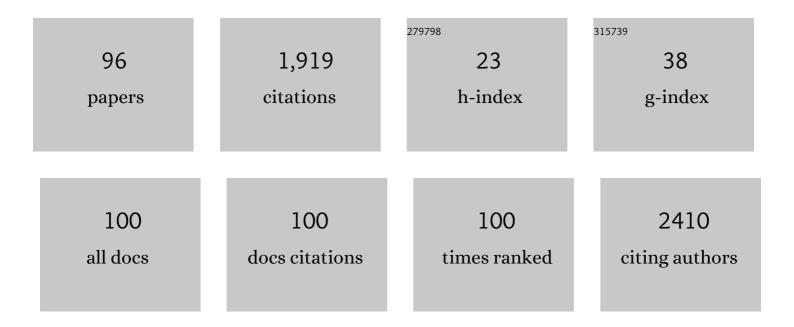
## Yoshitaka Aoki

List of Publications by Year in descending order

Source: https://exaly.com/author-pdf/293771/publications.pdf Version: 2024-02-01



#	Article	IF	CITATIONS
1	Development of Hydrogen-Permeable Metal Support Electrolysis Cells. ACS Applied Energy Materials, 2022, 5, 1385-1389.	5.1	3
2	High strength hydrogels enable dendrite-free Zn metal anodes and high-capacity Zn–MnO <sub>2</sub> batteries <i>via</i> a modified mechanical suppression effect. Journal of Materials Chemistry A, 2022, 10, 3122-3133.	10.3	17
3	High-corrosion-resistance mechanism of graphitized platelet-type carbon nanofibers in the OER in a concentrated alkaline electrolyte. Journal of Materials Chemistry A, 2022, 10, 8208-8217.	10.3	8
4	Single-phase La0.8Sr0.2Co1-Mn O3- electrocatalyst as a triple H+/O2-/e- conductor enabling high-performance intermediate-temperature water electrolysis. Journal of Materiomics, 2022, 8, 1020-1030.	5.7	5
5	Enhanced Performance of Protonic Solid Oxide Steam Electrolysis Cell of Zr-Rich Side BaZr <sub>0.6</sub> Ce <sub>0.2</sub> Y <sub>0.2</sub> O <sub>3â^î^</sub> Electrolyte with an Anode Functional Layer. ACS Omega, 2022, 7, 9944-9950.	3.5	4
6	Design of anode functional layers for protonic solid oxide electrolysis cells. Journal of Materials Chemistry A, 2022, 10, 15719-15730.	10.3	8
7	La <sub>0.8</sub> Sr <sub>0.2</sub> Co <sub>1-x</sub> Ni <i><sub>x</sub></i> O <sub>3-Î</sub> as the Efficient Triple Conductor Air Electrode for Protonic Ceramic Cells. ACS Applied Energy Materials, 2021, 4, 554-563.	5.1	34
8	The effect of an anode functional layer on the steam electrolysis performances of protonic solid oxide cells. Journal of Materials Chemistry A, 2021, 9, 14032-14042.	10.3	21
9	<i>In Situ</i> Activation of a Manganese Perovskite Oxygen Reduction Catalyst in Concentrated Alkaline Media. Journal of the American Chemical Society, 2021, 143, 6505-6515.	13.7	25
10	Highly Active and Durable FeNiCo Oxyhydroxide Oxygen Evolution Reaction Electrocatalysts Derived from Fluoride Precursors. ACS Sustainable Chemistry and Engineering, 2021, 9, 9465-9473.	6.7	16
11	Metal/Oxide Heterojunction Boosts Fuel Cell Cathode Reaction at Low Temperatures. Advanced Energy Materials, 2021, 11, 2102025.	19.5	16
12	Formation of Mobile Hydridic Defects in Zirconium Nitride Films with n-Type Semiconductor Properties. ACS Applied Electronic Materials, 2021, 3, 3980-3989.	4.3	6
13	Slippery Liquid-Infused Porous Surfaces on Aluminum for Corrosion Protection with Improved Self-Healing Ability. ACS Applied Materials & amp; Interfaces, 2021, 13, 45089-45096.	8.0	20
14	Hydrogen permeability of metal nitrides membranes with hydridic defects. Denki Kagaku, 2021, 89, 262-267.	0.0	1
15	A lithiophilic carbon scroll as a Li metal host with low tortuosity design and "Dead Li―self-cleaning capability. Journal of Materials Chemistry A, 2021, 9, 13332-13343.	10.3	15
16	Catalytic activity of graphene-covered non-noble metals governed by proton penetration in electrochemical hydrogen evolution reaction. Nature Communications, 2021, 12, 203.	12.8	77
17	Fluorineâ€Free Slippery Liquidâ€Infused Porous Surfaces Prepared Using Hierarchically Porous Aluminum. Physica Status Solidi (A) Applications and Materials Science, 2020, 217, 1900836.	1.8	10
18	Proton Pumping Boosts Energy Conversion in Hydrogen-Permeable Metal-Supported Protonic Fuel Cells. ACS Applied Energy Materials, 2020, 3, 1222-1234.	5.1	20

#	Article	IF	CITATIONS
19	A widely applicable strategy to convert fabrics into lithiophilic textile current collector for dendrite-free and high-rate capable lithium metal anode. Chemical Engineering Journal, 2020, 388, 124256.	12.7	27
20	In Situ Activation of Anodized Ni–Fe Alloys for the Oxygen Evolution Reaction in Alkaline Media. ACS Applied Energy Materials, 2020, 3, 12316-12326.	5.1	23
21	Compositional variations in anodic nanotubes/nanopores formed on Fe 100, 110 and 111 single crystals. Electrochimica Acta, 2020, 364, 137316.	5.2	4
22	Characterization of Dark-Colored Nanoporous Anodic Films on Zinc. Coatings, 2020, 10, 1014.	2.6	5
23	Mixed proton–electron–oxide ion triple conducting manganite as an efficient cobalt-free cathode for protonic ceramic fuel cells. Journal of Materials Chemistry A, 2020, 8, 11043-11055.	10.3	64
24	Highly Durable Oxygen Evolution Reaction Catalyst: Amorphous Oxyhydroxide Derived from Brownmillerite-Type Ca <sub>2</sub> FeCoO <sub>5</sub> . ACS Applied Energy Materials, 2020, 3, 5269-5276.	5.1	10
25	Long-term durability of platelet-type carbon nanofibers for OER and ORR in highly alkaline media. Applied Catalysis A: General, 2020, 597, 117555.	4.3	23
26	Spinel-Type Metal Oxide Nanoparticles Supported on Platelet-Type Carbon Nanofibers as a Bifunctional Catalyst for Oxygen Evolution Reaction and Oxygen Reduction Reaction. Electrochemistry, 2020, 88, 566-573.	1.4	5
27	Activation of Catalytically Active Edge-Sharing Domains in Ca <sub>2</sub> FeCoO <sub>5</sub> for Oxygen Evolution Reaction in Highly Alkaline Media. ACS Applied Materials & Interfaces, 2019, 11, 28823-28829.	8.0	25
28	Ultra-rapid formation of crystalline anatase TiO2 films highly doped with substrate species by a cathodic deposition method. Electrochemistry Communications, 2019, 108, 106561.	4.7	5
29	Incorporation of Bulk Proton Carriers in Cubic Perovskite Manganite Driven by Interplays of Oxygen and Manganese Redox. Chemistry of Materials, 2019, 31, 8383-8393.	6.7	26
30	High dispersion and oxygen reduction reaction activity of Co <sub>3</sub> O <sub>4</sub> nanoparticles on platelet-type carbon nanofibers. RSC Advances, 2019, 9, 3726-3733.	3.6	9
31	Heteroatom-doped porous carbon with tunable pore structure and high specific surface area for high performance supercapacitors. Electrochimica Acta, 2019, 314, 173-187.	5.2	51
32	High-valence-state manganate( <scp>v</scp> ) Ba <sub>3</sub> Mn <sub>2</sub> O <sub>8</sub> as an efficient anode of a proton-conducting solid oxide steam electrolyzer. Inorganic Chemistry Frontiers, 2019, 6, 1587-1597.	6.0	8
33	The role of tungsten species in the transition of anodic nanopores to nanotubes formed on iron alloyed with tungsten. Electrochimica Acta, 2019, 309, 274-282.	5.2	4
34	Exothermically Efficient Exfoliation of Biomass Cellulose to Value-Added N-Doped Hierarchical Porous Carbon for Oxygen Reduction Electrocatalyst. Industrial & Engineering Chemistry Research, 2019, 58, 3047-3059.	3.7	15
35	Employing a T-shirt template and variant of Schweizer's reagent for constructing a low-weight, flexible, hierarchically porous and textile-structured copper current collector for dendrite-suppressed Li metal. Journal of Materials Chemistry A, 2019, 7, 27066-27073.	10.3	7
36	Fabrication of Superoleophobic Surface on Stainless Steel by Hierarchical Surface Roughening and Organic Coating. ISIJ International, 2019, 59, 345-350.	1.4	12

#	Article	IF	CITATIONS
37	Vertically aligned carbon fibers as supporting scaffolds for phase change composites with anisotropic thermal conductivity and good shape stability. Journal of Materials Chemistry A, 2019, 7, 4934-4940.	10.3	86
38	Exâ€Situ Evidence for the Role of a Fluoride-Rich Layer Switching the Growth of Nanopores to Nanotubes: A Missing Piece of the Anodizing Puzzle. ChemElectroChem, 2018, 5, 570-570.	3.4	1
39	Enhanced hydrogen permeability of hafnium nitride nanocrystalline membranes by interfacial hydride conduction. Journal of Materials Chemistry A, 2018, 6, 2730-2741.	10.3	16
40	Starch-Derived Hierarchical Porous Carbon with Controlled Porosity for High Performance Supercapacitors. ACS Sustainable Chemistry and Engineering, 2018, 6, 7292-7303.	6.7	115
41	Electrochemical Oxidation of Hf–Nb Alloys as a Valuable Route to Prepare Mixed Oxides of Tailored Dielectric Properties. Advanced Electronic Materials, 2018, 4, 1800006.	5.1	17
42	Analysis of the Anode Reaction of Solid Oxide Electrolyzer Cells with BaZr <sub>0.4</sub> Ce <sub>0.4</sub> Y <sub>0.2</sub> O <sub>3-</sub> <i><sub>î´</sub></i> Electrolytes and Sm <sub>0.5</sub> Sr <sub>0.5</sub> CoO <sub>3-</sub> <i><sub>î´</sub></i> Anodes. Journal of the Electrochemical Society, 2018, 165, F342-F349.	2.9	23
43	Highly increased breakdown potential of anodic films on aluminum using a sealed porous layer. Journal of Solid State Electrochemistry, 2018, 22, 2073-2081.	2.5	4
44	Highâ€Efficiency Direct Ammonia Fuel Cells Based on BaZr <sub>0.1</sub> Ce <sub>0.7</sub> Y <sub>0.2</sub> O <sub>3â^'</sub> <i><sub>δ</sub></i> /Pd Oxideâ€Metal Junctions. Global Challenges, 2018, 2, 1700088.	3.6	25
45	Strong Lanthanoid Substitution Effect on Electrocatalytic Activity of Double-Perovskite-Type BaLnMn <sub>2</sub> O <sub>5</sub> (Ln = Y, Gd, Nd, and La) for Oxygen Reduction Reaction. Journal of Physical Chemistry C, 2018, 122, 7081-7087.	3.1	10
46	Ex Situ Evidence for the Role of a Fluorideâ€Rich Layer Switching the Growth of Nanopores to Nanotubes: A Missing Piece of the Anodizing Puzzle. ChemElectroChem, 2018, 5, 610-618.	3.4	19
47	La <sub>0.7</sub> Sr <sub>0.3</sub> Mn <sub>1–<i>x</i></sub> Ni <sub><i>x</i></sub> O <sub>3â<sup>^</sup>î<sup>&lt;</sup></sub> Elector for the Four-Electron Oxygen Reduction Reaction in Concentrated Alkaline Media. Journal of Physical Chemistry C, 2018, 122, 22301-22308.	trocatalys 3.1	sts 20
48	Nitrogen-doped porous carbon as-mediated by a facile solution combustion synthesis for supercapacitor and oxygen reduction electrocatalyst. Chemical Engineering Journal, 2018, 350, 278-289.	12.7	78
49	Evaluation of thin film fuel cells with Zr-rich BaZr <sub>x</sub> Ce <sub>0.8â^'x</sub> Y <sub>0.2</sub> O <sub>3â^'î</sub> electrolytes ( <i>x</i> ≥ 0.4) fabricated by a single-step reactive sintering method. RSC Advances, 2018, 8, 26309-26317.	3.6	20
50	Rapid and Repeatable Selfâ€Healing Superoleophobic Porous Aluminum Surface Using Infiltrated Liquid Healing Agent. Advanced Materials Interfaces, 2018, 5, 1800566.	3.7	17
51	Diffusion-controlled Growth of TiO <sub>2</sub> Mesoporous Anodic Films in Hot Phosphate/glycerol Electrolytes. Electrochemistry, 2018, 86, 184-189.	1.4	1
52	Anodizing for Photocatalysts. Hyomen Gijutsu/Journal of the Surface Finishing Society of Japan, 2018, 69, 609-612.	0.2	0
53	High Efficiency Hydrogen Membrane Fuel Cells with BaCe0.8Y0.2O3-ÎElectrolyte Thin Films and Pd1-xAgxSolid Anodes. Journal of the Electrochemical Society, 2017, 164, F577-F581.	2.9	1
54	Brownmilleriteâ€ŧype Ca <sub>2</sub> FeCoO <sub>5</sub> as a Practicable Oxygen Evolution Reaction Catalyst. ChemSusChem, 2017, 10, 2864-2868.	6.8	50

#	Article	IF	CITATIONS
55	Hydrogen separation by nanocrystalline titanium nitride membranes with high hydride ion conductivity. Nature Energy, 2017, 2, 786-794.	39.5	40
56	Co <sub>9</sub> S <sub>8</sub> Nanoparticles Incorporated in Hierarchically Porous 3D Few-Layer Graphene-Like Carbon with S,N-Doping as Superior Electrocatalyst for Oxygen Reduction Reaction. Particle and Particle Systems Characterization, 2017, 34, 1700296.	2.3	29
57	Brownmillerite-type Ca2 FeCoO5 as a Practicable Oxygen Evolution Reaction Catalyst. ChemSusChem, 2017, 10, 2841-2841.	6.8	5
58	Low-Temperature Oxygen Storage of Cr <sup>IV</sup> –Cr <sup>V</sup> Mixed-Valence YCr <sub>1–<i>x</i></sub> P <sub><i>x</i></sub> O <sub>4â^îÎ</sub> Driven by Local Condensation around Oxygen-Deficient Orthochromite. Journal of the American Chemical Society, 2017, 139, 11197-11206.	13.7	8
59	Nitrogenâ€Doped Hierarchical Porous Carbon Architecture Incorporated with Cobalt Nanoparticles and Carbon Nanotubes as Efficient Electrocatalyst for Oxygen Reduction Reaction. Advanced Materials Interfaces, 2017, 4, 1700583.	3.7	21
60	Growth of Barrier Type Anodic Film on Magnesium in Ethylene Glycol-Water Mixed Electrolytes Containing Fluoride and Phosphate. Materials Transactions, 2016, 57, 1552-1559.	1.2	3
61	Electrochemical Impedance Spectroscopy of High-Efficiency Hydrogen Membrane Fuel Cells Based on Sputter-Deposited BaCe <sub>0.8</sub> Y <sub>0.2</sub> O <sub>3â~î^</sub> Thin Films. Journal of Physical Chemistry C, 2016, 120, 15976-15985.	3.1	20
62	Fabrication of a resistive switching gallium oxide thin film with a tailored gallium valence state and oxygen deficiency by rf cosputtering process. RSC Advances, 2016, 6, 8964-8970.	3.6	24
63	Redox-induced proton insertion and desertion of zircon-type neodymium chromate(V). Solid State lonics, 2016, 285, 175-179.	2.7	1
64	GDOES Depth Profile Analysis of Interfacial Enrichment of Copper during Anodizing of Al-Cu Alloy. Hyomen Gijutsu/Journal of the Surface Finishing Society of Japan, 2015, 66, 670-672.	0.2	1
65	Corrosion protection of iron using porous anodic oxide/conducting polymer composite coatings. Faraday Discussions, 2015, 180, 479-493.	3.2	15
66	Highly durable platelet carbon nanofiber-supported platinum catalysts for the oxygen reduction reaction. Carbon, 2015, 87, 1-9.	10.3	23
67	Formation and field-assisted dissolution of anodic films on iron in fluoride-containing organic electrolyte. Electrochimica Acta, 2015, 151, 363-369.	5.2	23
68	Highly Enhanced Corrosion Resistance of Stainless Steel by Sol-Gel Layer-by-Layer Aluminosilicate Thin Coatings. Journal of the Electrochemical Society, 2014, 161, C57-C61.	2.9	22
69	Fabrication of superoleophobic hierarchical surfaces for low-surface-tension liquids. RSC Advances, 2014, 4, 30927.	3.6	38
70	Bulk mixed ion electron conduction in amorphous gallium oxide causes memristive behaviour. Nature Communications, 2014, 5, 3473.	12.8	119
71	Electrochemical Analysis of Hydrogen Membrane Fuel Cells with Amorphous Zirconium Phosphate Thin Film Electrolyte. Electrochemistry, 2014, 82, 859-864.	1.4	3
72	High Proton Conductivity in Anodic ZrO2-WO3-SiO2 Nanofilms. ECS Transactions, 2013, 50, 193-201.	0.5	0

#	Article	IF	CITATIONS
73	Compositional Dependence of the Proton Conductivity of Anodic ZrO2-WO3-SiO2Nanofilms at Intermediate Temperatures. Journal of the Electrochemical Society, 2013, 160, F1096-F1102.	2.9	4
74	Formation and Dielectric Properties of Anodic Films Formed on Ta-W Alloys at Various Formation Voltages. Electrochemistry, 2013, 81, 840-844.	1.4	2
75	Percolative proton conductivity of sol–gel derived amorphous aluminosilicate thin films. Physical Chemistry Chemical Physics, 2012, 14, 2735.	2.8	4
76	Thickness dependence of proton conductivity of anodic ZrO2–WO3–SiO2 nanofilms. Journal of Power Sources, 2012, 205, 194-200.	7.8	11
77	Finite Size Effect of Proton-Conductivity of Amorphous Silicate Thin Films Based on Mesoscopic Fluctuation of Glass Network. Journal of the American Chemical Society, 2011, 133, 3471-3479.	13.7	22
78	Fabrication of Super-Oil-Repellent Dual Pillar Surfaces with Optimized Pillar Intervals. Langmuir, 2011, 27, 11752-11756.	3.5	76
79	Formation and dielectric properties of anodic oxide films on Zr–Al alloys. Journal of Solid State Electrochemistry, 2011, 15, 2221-2229.	2.5	9
80	Power-law scaling of proton conductivity in amorphous silicate thin films. Solid State Ionics, 2011, 192, 93-96.	2.7	0
81	Superhydrophobic hierarchical surfaces fabricated by anodizing of oblique angle deposited Al–Nb alloy columnar films. Applied Surface Science, 2011, 257, 8282-8288.	6.1	19
82	Influence of Phosphate Concentration on Plasma Electrolytic Oxidation of AZ80 Magnesium Alloy in Alkaline Aluminate Solution. Materials Transactions, 2010, 51, 94-102.	1.2	24
83	Galvanostatic Growth of Nanoporous Anodic Films on Iron in Ammonium Fluorideâ^'Ethylene Glycol Electrolytes with Different Water Contents. Journal of Physical Chemistry C, 2010, 114, 18853-18859.	3.1	62
84	Thickness-Induced Proton-Conductivity Transition in Amorphous Zirconium Phosphate Thin Films. Chemistry of Materials, 2010, 22, 5528-5536.	6.7	15
85	Size-Scaling of Proton Conductivity in Amorphous Aluminosilicate Acid Thin Films. Journal of the American Chemical Society, 2009, 131, 14399-14406.	13.7	26
86	Formation of Porous Aluminum Films with Isolated Columnar Structure Using Physical Vapor Deposition for Medium-Voltage and High-voltage Capacitors. Hyomen Gijutsu/Journal of the Surface Finishing Society of Japan, 2009, 60, 166-169.	0.2	1
87	Efficient Proton Conductivity of Gasâ€Tight Nanomembranes of Silicaâ€Based Double Oxides. Advanced Materials, 2008, 20, 4387-4393.	21.0	22
88	Determination of Surface Area and Porosity of Small, Nanometer-Thick Films by Quartz Crystal Microbalance Measurement of Gas Adsorption. Journal of Physical Chemistry B, 2008, 112, 14578-14582.	2.6	5
89	Thickness Dependence of Proton Conductivity of Amorphous Aluminosilicate Nanofilm. Electrochemical and Solid-State Letters, 2008, 11, P13.	2.2	10
90	Efficient proton conduction in dry nanofilms of amorphous aluminosilicate. Chemical Communications, 2007, , 2396.	4.1	12

#	Article	IF	CITATIONS
91	Reducing Gas Sensing Based on the Redox Interconversion of Neodymium (III) Chromate(V). Chemistry Letters, 2004, 33, 992-993.	1.3	1
92	Interconversion between Rare-Earth Metal(III) Chromates(V) and Low-Crystalline Phases by Reduction with Methanol and Oxidation in Air. Chemistry of Materials, 2003, 15, 2419-2428.	6.7	6
93	Synthesis of C/B 4 C composites from sugar-boric acid mixed solutions. Molecular Crystals and Liquid Crystals, 2002, 386, 15-20.	0.9	5
94	Synthesis, structure and defects of rare earth chromates(V), RE0.9CrO3.85 (RE = Gd, Yb and Y). Journal of Materials Chemistry, 2001, 11, 1458-1464.	6.7	7
95	The electronic and magnetic properties of LaCrO4 and Nd1 â^' xCaxCrO4 (x = 0–0.2) and the conduction mechanism. Journal of Materials Chemistry, 2001, 11, 1214-1221.	6.7	21
96	Characterization of LaCrO4and NdCrO4by XRD, Raman Spectroscopy, and ab Initio Molecular Orbital Calculations. Bulletin of the Chemical Society of Japan, 2000, 73, 1197-1203.	3.2	28